1 # Genome editing in mitochondria corrects a pathogenic

2 # mtDNA mutation *in vivo*

3

4 Payam A. Gammage[1]*, Carlo Viscomi[1], Marie-Lune Simard[2], Ana S.H. Costa[3], Edoardo

5 Gaude[3], Christopher A. Powell[1], Lindsey Van Haute[1], Beverly J. McCann[1], Pedro

6 Rebelo-Guiomar[1,4], Raffaele Cerutti[1], Lei Zhang[5], Edward J. Rebar[5], Massimo Zeviani[1],

7 Christian Frezza[3], James B. Stewart[2] and Michal Minczuk[1]*

8

9 [1] MRC Mitochondrial Biology Unit, University of Cambridge, Cambridge, UK

10 [2] Max Planck Institute for Biology of Ageing, Cologne, Germany

11 [3] MRC Cancer Unit, University of Cambridge, Cambridge, UK

12 [4] Graduate Program in Areas of Basic and Applied Biology (GABBA), University of

13   Porto, Porto, Portugal

14 [5] Sangamo Therapeutics Inc., Richmond, California, USA

15

16

17 *To whom correspondence should be addressed:

18 payam.gammage@mrc-mbu.cam.ac.uk, michal.minczuk@mrc-mbu.cam.ac.uk

19

20

21   [Introductory paragraph]

22

23   Mutations of the mitochondrial genome (mtDNA) underlie a significant portion of

24   mitochondrial disease burden. These disorders are currently incurable and effectively

25   untreatable, with heterogeneous penetrance, presentation and prognosis. To address

26   the lack of effective treatment for these disorders, we exploited a recently developed

27   mouse model that recapitulates common molecular features of heteroplasmic mtDNA

28   disease in cardiac tissue, the m.5024C>T tRNA[ALA] mouse. Through application of a

29   programmable nuclease therapy approach, using systemically administered,

30   mitochondrially targeted zinc finger-nucleases (mtZFNs) delivered by adeno-associated

31   virus, we induced specific elimination of mutant mtDNA across the heart, coupled to a

32   reversion of molecular and biochemical phenotypes. These findings constitute proof-of-

33   principle that mtDNA heteroplasmy correction using programmable nucleases could

34   provide a therapeutic route for heteroplasmic mitochondrial diseases of diverse genetic

35   origin.

36

37   [Introduction]

38

39   Mitochondrial diseases are a broad group of hereditary, multi-system disorders, a

40   substantial portion of which are transmitted through mutations of mitochondrial DNA

41   (mtDNA) with minimum prevalence of 1 in 5,000 adults [1]. Human mtDNA is a small,

42   double-stranded, multi-copy genome present at ~ 100 – 10,000 copies per cell [2]. In the

43   disease state, mutated mtDNA often co-exists with wild-type mtDNA in heteroplasmy,

44   and disease severity in conditions caused by heteroplasmic mtDNA mutations

45   correlates with mutation load [3]. A threshold effect, where > 60% mutant mtDNA load

46   must be exceeded before symptoms manifest, is a definitive feature of heteroplasmic

47   mtDNA diseases, and attempts to shift the heteroplasmic ratio below this threshold have

48   driven much research towards treatment of these incurable and essentially untreatable

49   disorders. One such approach relies on directed nucleolysis of mtDNA using, among

50   other programmable genome engineering tools, mitochondrially targeted zinc finger-

51   nucleases (mtZFNs) [4-6]. Because mammalian mitochondria lack efficient DNA double-

52   strand break (DSB) repair pathways [7], selective introduction of DSBs into mutant

53   mtDNA leads to rapid degradation of these molecules by components of the mtDNA

54   replisome [8]. As mtDNA copy number is maintained at a cell type-specific steady-state

55   level, selective elimination of mutant mtDNA stimulates replication of the remaining

56   mtDNA pool, eliciting shifts in the heteroplasmic ratio.

57   In previous work, we have described methods for delivery of zinc finger proteins

58   (ZFPs) to mitochondria in cultured cells [9,10] and the assembly and function of efficient

59   mtZFN architectures, capable of producing large heteroplasmic shifts that result in

60   phenotype rescue of patient-derived cell cultures [5,11-13]. Using the first available mouse

61   model of heteroplasmic mitochondrial disease, bearing the point mutation m.5024C>T

62   in mitochondrial tRNA^{ALA} (mt-tRNA^{ALA}), which faithfully recapitulates key molecular

63   features of mitochondrial disorders in cardiac tissue [14], we now demonstrate efficient

64   manipulation of mtDNA heteroplasmy with concomitant rescue of molecular and

65   biochemical phenotypes across the heart following delivery of mtZFNs by systemically

66   administered adeno-associated virus (AAV).

67

68   [Results]

69

70 In the context of second generation tail-tail mtZFN architectures (mtZFN[2G]) shown to be

71 efficacious in previous work [5,15], we set out to generate pairs of zinc finger proteins

72 (ZFP) with single nucleotide binding specificity for m.5024C>T. As this site in the mouse

73 mtDNA is challenging for ZFPs, a selection of targeting strategies with varying numbers

74 of zinc finger motifs, spacer region lengths and additional linkers were employed.

75 Assembly of candidate ZFPs yielded a library (**Fig. S1A** and **Table S1**) consisting of 24

76 unique ZFPs targeting the m.5024C>T site, referred to as mutant-specific monomer

77 (MTM), and a single partner ZFP targeting an adjacent sequence on the opposite

78 strand, referred to as wild-type-specific monomer 1 (WTM1). These constructs were

79 subjected to several rounds of screening in mouse embryonic fibroblasts (MEFs)

80 bearing ~ 65% m.5024C>T to assess heteroplasmy shifting activity (**Fig. S1B**). These

81 screens identified consistent, specific activity of pairing MTM25/WTM1 (**Fig. S1C** and

82 **Fig. 1A**), which produced a shift of ~ 20%, from 65% to 45% m.5024C>T in the MEF

83 cell line as determined by pyrosequencing (**Fig. 1B**). We additionally confirmed

84 exclusive mitochondrial localization of MTM25 and WTM1 in MEF cells (**Fig. S2**), and

85 then selected this pair for *in vivo* experiments.

86   MTM25 and WTM1 mtZFN monomers were encoded in separate viral genomes

87 and encapsidated within the cardiac-tropic, engineered AAV9.45 serotype (**Fig. 1C**) [16].

88 Following tail-vein administration of $5*10^{12}$ viral genomes (vg) per monomer per mouse,

89 robust expression of MTM25 and WTM1 in total mouse heart tissue was detected by

90 western blotting (**Fig. 1D**). Despite equal quantities of injected viral genomes, lower

91 expression levels of WTM1 were consistently detected, possibly due to lower stability of

92 the translated protein. Next, various doses of mtZFN-AAV9.45 were administered into

93 mt-tRNA[ALA] animals harbouring m.5024C>T heteroplasmy ranging from 44 % - 81 %

94 (**Table S2**). As only minimal variance in heteroplasmy is observed between tissues of

95   the m.5024C>T mouse[13], mtDNA heteroplasmy is assessed by comparison of

96   pyrosequencing data, expressed as the change (Δ) between ear punch genotype (E)

97   determined at two weeks of age (prior to experimental intervention) and post-mortem

98   heart genotype (H). Analysis of animals at 65 days post-injection revealed specific

99   elimination of the m.5024C>T mutant mtDNA in mtZFN-treated mice, but not in vehicle-

100   or single monomer-injected controls (**Fig. 1E**). The extent to which heteroplasmy was

101   altered by mtZFN treatment followed a biphasic AAV dose-dependent trend, with the

102   intermediate dose ($5*10^{12}$ vg) being the most efficient in eliminating m.5024C>T mutant

103   mtDNA (**Fig. 1E**). The lowest ($1*10^{12}$ vg) dose did not result in heteroplasmy shifts (**Fig.**

104   **1E**), due to insufficient concentration of mtZFNs and mosaic transduction of the targeted

105   tissue by AAV (**Fig. S3**). The highest dose ($1*10^{13}$ vg) exhibited diminished

106   heteroplasmy shifting activity compared with the intermediate dose ($5*10^{12}$ vg), likely

107   due to mitochondrial off-target effects resulting in partial mtDNA copy number

108   depletions, which are not observed when lower doses are administered (**Fig. 1F**). It is

109   unclear what effect, if any, these partial depletions of mtDNA copy number could exert

110   over time, however this lattermost result is consistent with our previous observations [12],

111   underscoring the importance of fine-tuning mtZFN levels in mitochondria for efficient

112   mtDNA heteroplasmy modification. AAV9.45 transduction could not be detected in non-

113   cardiac tissues, and no shifts in heteroplasmy were detected in the liver at 65 days post-

114   injection, irrespective of viral dose (**Fig. S3**). As AAV transduction of post-mitotic

115   tissues, particularly in short-lived mammals, is essentially permanent, a time-

116   dependence of heteroplasmy shifting is expected. Accordingly, measurements of

117   mtDNA heteroplasmy over time in cardiac tissue demonstrate significant increases in

118   heteroplasmy shifting activity in the latest post-treatment time points (**Fig. S4**). Despite

119   the presence of two regions with significant homology to the mtDNA target site in the

120   nuclear genome, no evidence for off-target effects exerted by mtZFNs could be

121   detected at these sites (**Fig. S5A,B**), consistent with our previous reports of exclusive

122   mitochondrial localization of mtZFNs [5,9,10,12]. Additionally, no evidence for non-

123   homologous end-joining (NHEJ) at the target site in mtDNA could be detected,

124   confirming previous data that mtZFN-induced DNA DSBs do not result in NHEJ activity

125   (**Fig. S5C**) [12].

126   Having defined conditions within which a robust shift of m.5024C>T

127   heteroplasmy is achieved *in vivo*, we next addressed disease-relevant phenotype

128   correction in the model. A common feature of mt-tRNA mutations in mitochondrial

129   diseases, recapitulated in the tRNA^ALA mouse model [14], is the instability of mt-tRNA

130   molecules in proportion with mutant load (**Fig. 2A**) [17]. To assess the effects of mtZFN

131   treatment on the stability of mt-tRNA^ALA in the hearts of animals across the dosage

132   range, we used high-resolution northern blotting, which revealed a significant increase

133   in mt-tRNA^ALA steady-state levels (**Fig. 2B** and **Fig. S6**) that are proportional to

134   heteroplasmy shifts detected in these mice (average m.5024C>T heteroplasmy: control

135   71% pre-, 73% post-treatment; low AAV dose, 73% pre-, 71% post-treatment; medium

136   AAV dose, 73% pre-, 37% post-treatment; high AAV dose, 71% pre-, 40% post-

137   treatment) (**Fig. 1E** and **Table S2**) and consistent with previously reported data [14].

138   Depletions of mtDNA copy number associated with administration of high viral doses

139   (**Fig. 1F**), did not appear to impact recovery of mt-tRNA^ALA steady-state levels following

140   heteroplasmy shift (**Fig. 2B**). This agrees with previously published data that even

141   severe mtDNA depletion does not manifest in proportional changes of mitochondrial

142   RNA steady-state levels [18].

143   To assess the physiological effects of mt-tRNA^ALA molecular phenotype rescue,

144   we analyzed steady-state metabolite levels in cardiac tissue from mice with high

145   m.5024C>T mutant heteroplasmy treated with the intermediate viral titer ($5*10^{12}$ vg) and

146   heteroplasmy/age matched controls (**Table S2**). This analysis revealed an altered

147   metabolic signature in mtZFN treated mice (**Fig. 2C** and **Fig. S7**), demonstrating

148   significantly increased pyruvate levels (**Fig. 2D**) and significantly decreased lactate

149   levels (**Fig. 2E**) in treated mice, suggestive of a diminished reliance on glycolysis,

150   coupled to elevated aspartate levels (**Fig. 2F**) in treated mice, suggestive of improved

151   mitochondrial respiration [19]. These indicators of improved mitochondrial metabolism are

152   not observed in mice treated with the highest AAV dose (**Fig. S8**), which also exhibit

153   substantial copy number depletions (**Fig. 1F**). Due to phenotypic heterogeneity of mice

154   bearing high levels of mtDNA heteroplasmy, changes in gross cardiac function following

155   heteroplasmic shifts could not be assessed. Taken together, these data indicate that

156   partial m.5024C>T heteroplasmy shift (**Fig. 1E**) results in recovery of mt-tRNA^{ALA}

157   steady-state levels and rescue of mitochondrial function (**Fig. 2C-F**).

158

159   [Discussion]

160

161   Our previous reports on the use of mtZFN technology have demonstrated that these

162   programmable nucleases can target multiple genetic lesions, producing phenotypically

163   relevant shifts of mtDNA heteroplasmy in cellular models of mitochondrial dysfunction

164   [5,12,13]. Here, we have further demonstrated the flexibility and future potential of mtZFN

165   technology by targeting another heteroplasmic mutation in mouse mtDNA, m.5024C>T,

166   manipulating the heteroplasmy of this variant both *in vitro* and *in vivo* (**Fig. 1**)*,* which

167   results in molecular and physiological rescue of disease phenotypes in heart tissue

168   (**Fig. 2**).

169   Despite the time elapsed since mtDNA mutations were first associated with

170   human disease in the late 1980's [20,21], effective treatments for heteroplasmic

171   mitochondrial disease have not been forthcoming. Preventing the transmission of

172   mtDNA mutations through mitochondrial replacement therapy/mitochondrial donation

173   has gained traction [22,23], although given the nature of the mtDNA bottleneck [24], issues

174   surrounding carryover of mutant mtDNA [25], heterogeneous mitochondrial disease

175   presentation [26] and the subsequent lack of family history of mitochondrial disease in the

176   majority of new cases, these approaches can only be of limited use. More recently,

177   several intriguing molecular pathways to treatment of mitochondrial disease have been

178   defined and explored by a number of groups [27], however, hopes for clinically-relevant

179   therapy for heteroplasmic mitochondrial disease, thus far, remain unfulfilled [28]. The data

180   we describe in this letter, and those from Bacman *et al.* [29], constitute proof-of-principle

181   that somatic mitochondrial genome editing using programmable nucleases, in

182   combination with the ever-increasing collection of engineered, tissue-specific AAV

183   serotypes, may offer a potentially universal route to treatment for heteroplasmic

184   mitochondrial disease. Given the magnitude of *in vivo* heteroplasmy modification

185   demonstrated using these tools, total amelioration of clinical symptoms and/or halting of

186   disease progression could be expected. As such, this development has the potential to

187   transform the prospects of many mitochondrial disease patients, and further work

188   enabling the translation of these tools into effective medicines is vital.

189

190   [Data availability statement]

191

192 All NGS data generated in the present study are available from the BioProject database

193 using accession number PRJNA479953. All other datasets and materials are available

194 from the corresponding authors.

195

196

197

198

199 [Acknowledgements]

200

214

215 [Author Contributions]

231

232   [References]

233

234   1   Gorman, G. S. *et al.* Prevalence of nuclear and mitochondrial DNA mutations
235   related to adult mitochondrial disease. *Ann Neurol* **77**, 753-759,
236   doi:10.1002/ana.24362 (2015).
237   2   Wachsmuth, M., Hubner, A., Li, M., Madea, B. & Stoneking, M. Age-Related and
238   Heteroplasmy-Related Variation in Human mtDNA Copy Number. *Plos Genet* **12**,
239   e1005939, doi:10.1371/journal.pgen.1005939 (2016).
240   3   Gorman, G. S. *et al.* Mitochondrial diseases. *Nat Rev Dis Primers* **2**, 16080,
241   doi:10.1038/nrdp.2016.80 (2016).
242   4   Bacman, S. R., Williams, S. L., Pinto, M., Peralta, S. & Moraes, C. T. Specific
243   elimination of mutant mitochondrial genomes in patient-derived cells by
244   mitoTALENs. *Nat Med* **19**, 1111-1113, doi:10.1038/nm.3261 (2013).
245   5   Gammage, P. A., Rorbach, J., Vincent, A. I., Rebar, E. J. & Minczuk, M.
246   Mitochondrially targeted ZFNs for selective degradation of pathogenic

247   mitochondrial genomes bearing large-scale deletions or point mutations. *EMBO*
248   *Mol Med* **6**, 458-466, doi:10.1002/emmm.201303672 (2014).
249 6   Reddy, P. *et al.* Selective elimination of mitochondrial mutations in the germline
250   by genome editing. *Cell* **161**, 459-469, doi:10.1016/j.cell.2015.03.051 (2015).
251 7   Alexeyev, M., Shokolenko, I., Wilson, G. & LeDoux, S. The maintenance of
252   mitochondrial DNA integrity--critical analysis and update. *Cold Spring Harb*
253   *Perspect Biol* **5**, a012641, doi:10.1101/cshperspect.a012641 (2013).
254 8   Peeva, V. *et al.* Linear mitochondrial DNA is rapidly degraded by components of
255   the replication machinery. *Nat Commun* **9**, 1727, doi:10.1038/s41467-018-04131-
256   w (2018).
257 9   Minczuk, M., Papworth, M. A., Kolasinska, P., Murphy, M. P. & Klug, A.
258   Sequence-specific modification of mitochondrial DNA using a chimeric zinc finger
259   methylase. *Proc Natl Acad Sci U S A* **103**, 19689-19694 (2006).
260 10   Minczuk, M., Kolasinska-Zwierz, P., Murphy, M. P. & Papworth, M. A.
261   Construction and testing of engineered zinc-finger proteins for sequence-specific
262   modification of mtDNA. *Nat Protoc* **5**, 342-356, doi:10.1038/nprot.2009.245
263   (2010).
264 11   Minczuk, M., Papworth, M. A., Miller, J. C., Murphy, M. P. & Klug, A.
265   Development of a single-chain, quasi-dimeric zinc-finger nuclease for the
266   selective degradation of mutated human mitochondrial DNA. *Nucleic Acids Res*
267   **36**, 3926-3938, doi:10.1093/nar/gkn313 (2008).
268 12   Gammage, P. A. *et al.* Near-complete elimination of mutant mtDNA by iterative or
269   dynamic dose-controlled treatment with mtZFNs. *Nucleic Acids Res* **44**, 7804-
270   7816, doi:10.1093/nar/gkw676 (2016).
271 13   Gaude, E. *et al.* NADH Shuttling Couples Cytosolic Reductive Carboxylation of
272   Glutamine with Glycolysis in Cells with Mitochondrial Dysfunction. *Mol Cell* **69**,
273   581-593 e587, doi:10.1016/j.molcel.2018.01.034 (2018).
274 14   Kauppila, J. H. *et al.* A Phenotype-Driven Approach to Generate Mouse Models
275   with Pathogenic mtDNA Mutations Causing Mitochondrial Disease. *Cell Rep* **16**,
276   2980-2990, doi:10.1016/j.celrep.2016.08.037 (2016).
277 15   Gammage, P. A., Van Haute, L. & Minczuk, M. Engineered mtZFNs for
278   Manipulation of Human Mitochondrial DNA Heteroplasmy. *Methods Mol Biol*
279   **1351**, 145-162, doi:10.1007/978-1-4939-3040-1_11 (2016).
280 16   Pulicherla, N. *et al.* Engineering liver-detargeted AAV9 vectors for cardiac and
281   musculoskeletal gene transfer. *Mol Ther* **19**, 1070-1078, doi:10.1038/mt.2011.22
282   (2011).
283 17   Yarham, J. W., Elson, J. L., Blakely, E. L., McFarland, R. & Taylor, R. W.
284   Mitochondrial tRNA mutations and disease. *Wiley Interdiscip Rev RNA* **1**, 304-
285   324, doi:10.1002/wrna.27 (2010).
286 18   Jazayeri, M. *et al.* Inducible expression of a dominant negative DNA polymerase-
287   gamma depletes mitochondrial DNA and produces a rho0 phenotype. *J Biol*
288   *Chem* **278**, 9823-9830 (2003).
289 19   Birsoy, K. *et al.* An Essential Role of the Mitochondrial Electron Transport Chain
290   in Cell Proliferation Is to Enable Aspartate Synthesis. *Cell* **162**, 540-551,
291   doi:10.1016/j.cell.2015.07.016 (2015).
292 20   Holt, I. J., Harding, A. E. & Morgan-Hughes, J. A. Deletions of muscle
293   mitochondrial DNA in patients with mitochondrial myopathies. *Nature* **331**, 717-
294   719, doi:10.1038/331717a0 (1988).
295 21   Wallace, D. C. *et al.* Mitochondrial DNA mutation associated with Leber's
296   hereditary optic neuropathy. *Science* **242**, 1427-1430 (1988).

297   22   Craven, L. *et al.* Pronuclear transfer in human embryos to prevent transmission
298   of mitochondrial DNA disease. *Nature* **465**, 82-85, doi:10.1038/nature08958
299   (2010).
300   23   Tachibana, M. *et al.* Towards germline gene therapy of inherited mitochondrial
301   diseases. *Nature* **493**, 627-631, doi:10.1038/nature11647 (2013).
302   24   Floros, V. I. *et al.* Segregation of mitochondrial DNA heteroplasmy through a
303   developmental genetic bottleneck in human embryos. *Nat Cell Biol* **20**, 144-151,
304   doi:10.1038/s41556-017-0017-8 (2018).
305   25   Yamada, M. *et al.* Genetic Drift Can Compromise Mitochondrial Replacement by
306   Nuclear Transfer in Human Oocytes. *Cell Stem Cell* **18**, 749-754,
307   doi:10.1016/j.stem.2016.04.001 (2016).
308   26   Vafai, S. B. & Mootha, V. K. Mitochondrial disorders as windows into an ancient
309   organelle. *Nature* **491**, 374-383, doi:10.1038/nature11707 (2012).
310   27   Viscomi, C., Bottani, E. & Zeviani, M. Emerging concepts in the therapy of
311   mitochondrial disease. *Biochim Biophys Acta* **1847**, 544-557,
312   doi:10.1016/j.bbabio.2015.03.001 (2015).
313   28   Pfeffer, G. *et al.* New treatments for mitochondrial disease-no time to drop our
314   standards. *Nat Rev Neurol* **9**, 474-481, doi:10.1038/nrneurol.2013.129 (2013).
315   29   Bacman, S. R. et al. MitoTALEN reduces mutant mtDNA load and restores
316   tRNAAla levels in a mouse model of heteroplasmic mtDNA mutation. *Nature*
317   *Medicine* **in press** (2018). (back-to-back submission)
318
319

320   [Figure Legends]

321

322   **Figure 1**. Strategy to eliminate m.5024C>T and *in vivo* mtDNA heteroplasmy

323   modification. **A** Illustration of mtZFN strategy. A wild-type specific monomer (WTM1),

324   bind upstream of m.5024 in wild-type and mutant genomes; a mutant specific monomer

325   (MTM25) binds preferentially to the mutated site. Dimerization of obligatory

326   heterodimeric *Fok*I domains produces DNA double-stand breaks resulting in specific

327   depletion of mutant mtDNA. **B** Pyrosequencing of m.5024C>T heteroplasmy from MEFs

328   transfected with controls or MTM25/WTM1 at differing concentrations facilitated by

329   tetracycline-sensitive HHR [12]. Change (Δ) in m.5024C>T heteroplasmy is plotted. utZFN

330   is a mtZFN that does not have a target site in mouse mtDNA [12]. n = 5 (mtZFN, low

331   expression), 8 (mtZFN, high expression), 4 (all other conditions) biologically

332   independent cell cultures (**Table S2**). Error bars indicate SD. Statistical analysis

333   performed: two-tailed Student's t-test. Vehicle/mtZFN low expression p = 0.000021,

334   vehicle/mtZFN high expression p = 0.000083. Measure of center is the mean. **C**

335   Scheme of *in vivo* experiments. MTM25 and WTM1 are encoded in separate AAV

336   genomes, encapsidated in AAV9.45 then simultaneously administered by tail-vein (TV)

337   injection. Animals are sacrificed at 65 days post-injection. **D** Western blot of total heart

338   protein from animals injected with $5*10^{12}$ vg MTM25 and/or WTM1. Both proteins

339   include the HA tag and are differentiated by molecular weight. This blot was performed

340   twice with similar results. Raw data are available for this panel (**Fig. S9**). **E**

341   Pyrosequencing of m.5024C>T heteroplasmy from ear [E] and heart [H] total DNA.

342   Change (Δ) in m.5024C>T is plotted. n = 20 (vehicle), 3 (WTM1 only), 4 (all other

343   conditions) animals (**Table S2**). Error bars indicate SEM. Statistical analysis performed:

344   two-tailed Student's t-test. Vehicle/intermediate dose p < 0.00001, Vehicle/high dose p

345   < 0.00001. Measure of center is the mean. **F** Assessment of mtDNA copy number by

346   qPCR. n = 8 (vehicle), 4 (all other conditions) animals (**Table S2**). Error bars indicate

347   SEM. Statistical analysis performed: two-tailed Student's t-test p = 0.007931. Measure

348   of center is the mean.

349

350   **Figure 2**. Reduction of m.5024C>T mtDNA heteroplasmy results in phenotype rescue.

351   **A** Illustration of mt-tRNA^{ALA} bearing the m.5024C>T mutation. Given the nature and

352   position of this mutation, transcribed tRNA molecules containing the mutation mispair

353   are unlikely to fold correctly or be aminoacylated, resulting in reduced steady-state

354   levels of mt-tRNA^{ALA} at high levels of m.5024C>T heteroplasmy [14]. **B** Quantification of

355   high-resolution northern blot data from total heart RNA extracts. mt-tRNA^{ALA} and mt-

356   tRNA^{CYS} abundance was normalized to 5S rRNA. n = 8 (vehicle), 4 (all other conditions)

357   animals (**Table S2**). Error bars indicate SEM. Statistical analysis performed: two-tailed

358   Student's t-test. Vehicle/intermediate dose p < 0.00001, vehicle/high dose p = 0.00011.

359   Measure of center is the mean. **C** Principal component analysis (PCA) plot of

360   metabolomic data for intermediate dose AAV-treated mice and age/initial heteroplasmy-

361   matched controls acquired by LC-MS (**Table S2**). n = 3 (vehicle), 4 (AAV) animals. **D**

362   Total metabolite levels of pyruvate from samples measured in C. n = 3 (vehicle), 4

363   (AAV) animals. Error bars indicate SEM. Statistical analysis performed: one-tailed

364   Student's t-test. p = 0.046403. Measure of center is the mean. **E** Total metabolite levels

365   of lactate from samples measured in C. n = 3 (vehicle), 4 (AAV) animals. Error bars

366   indicate SEM. Statistical analysis performed: one-tailed Student's t-test. p = 0.03505.

367   Measure of center is the mean. **E** Total metabolite levels of aspartate from samples

368   measured in C. Error bars indicate SEM. n = 3 (vehicle), 4 (AAV) animals. Measure of

369   center is the mean

370

371

372

373   [Online Methods]

374

375   *Constructs, plasmids and viral vectors*

376   All mtZFN architectures used were as reported for second generation mtZFN

377   (mtZFN²ᴳ), with the exception of the ZFP domains [5,15]. The MTM(n)_T2A_WTM1

378   m.5024C>T candidate library was cloned by insertion of the MTM ZFP domains

379   upstream of *Fok*I(+) between 5' *EcoR*I and 3' *BamH*I restriction sites. This product was

380   then PCR amplified to include a 5' *Apa*I site and remove the 3' stop codon while also

381   incorporating a T2A sequence and 3' *Xho*I site. This fragment was then cloned into

382   pcmCherry (Addgene 62803) using *Apa*I/*Xho*I sites. The WTM1 ZFP was separately

383   cloned upstream of *Fok*I(-) in the pcmCherry_3k19 vector (Addgene 104499)

384   incorporating the 3' hammerhead ribozyme (HHR) using 5' *EcoR*I and 3' *BamH*I sites,

385   and the resulting product was PCR amplified to include 5' *Xho*I and 3' *Afl*II sites allowing

386   cloning downstream of MTM(n) variants. MTM25(+) and WTM1(-) monomers were

387   cloned into separate pcmCherry and pTracer vectors as described previously [15]. Vector

388   construction of mtZFNs intended for AAV production was achieved by PCR

389   amplification of MTM25(+)_HHR and WTM1(-)_HHR transgenes, incorporating 5' *Eag*I

390   and 3' *Bgl*II sites. These products were then cloned into rAAV2-CMV between 5' *Eag*I

391   and 3' *BamH*I sites. The FLAG epitope tag of WTM1(-) was replaced with a

392   hemagglutinin (HA) tag at the same position in the WTM1(-) open reading frame by

393   PCR. The resulting plasmids were used to generate recombinant AAV2/9.45-CMV-

394   MTM25 and AAV2/9.45-CMV-WTM1 viral particles at the UNC Gene Therapy Center,

395   Vector Core Facility (Chapel Hill, NC). The 3K19 hammerhead ribozyme (HHR)

396   sequence [30] was incorporated into mtZFN-AAV9.45 constructs to allow ubiquitous

397   expression of the transgene from CMV while limiting the expression level, allowing

398   administration of the high viral titers required to ensure effective co-transduction of cells

399   in the targeted tissue without inducing large mtDNA copy number depletions.

400

401   *Maintenance, transfection and fluorescence activated cell sorting of cell cultures*

402   Wild-type and m.5024C>T mouse embryonic fibroblast (MEF) cell lines were cultured in

403   Dulbecco's Modified Eagle's Medium (DMEM) containing 2 mM L-glutamine, 110 mg/L

404   sodium pyruvate (Life Technologies) and 10% FCS (PAA Laboratories). Cells were

405   transfected by electroporation using Nucleofector II apparatus (Lonza) using a MEF1 kit

406   and T20 program. Fluorescence activated cell sorting (FACS) was performed as

407   described previously [15]. Control of mtZFN expression was achieved through titration of

408   tetracycline into culture media, controlling the rate of HHR autocatalysis as described

409   previously [12].

410

411   *Use of animal models*

412   All animal experiments were carried out in accordance with the UK Animals (Scientific

413   Procedures) Act 1986 (PPL70/7538) and EU Directive 2010/63/EU. The C57BL/6j-

414   tRNA[ALA] mice used in this study were housed from one to four per cage in a

415   temperature controlled (21°C) room with a 12 h light-dark cycle and 60% relative

416   humidity. The experimental design included only male mice between 2 to 8 months of

417   age harboring 44 % - 81 % m.5024C>T heteroplasmy (20 Vehicle, 7 Single Monomer, 4

418   per mtZFN-AAV9.45 dosage) (**Table S1**). Treatments of vehicle (1 x PBS, 350 mM

419   NaCl, 5% w/v D-sorbitol) and AAVs were administered by tail vein injection.

420

421 *Protein extraction and quantitation*

422 For cultured cells, total cellular protein was extracted as described previously [12]. For

423 mouse heart tissue, 50 mg was homogenised in RIPA buffer (150 mM NaCl, 50 mM Tris

424 pH 8, 1% (v/v) Triton X-100, 0.5% (v/v) deoxycholate, 0.1% (v/v) SDS) using a

425 gentleMACS dissociator (Miltenyi). The resulting homogenate was centrifuged at 10,000

426 x g at 4C for 10 minutes, supernatant was then recovered and centrifuged at 10,000 x g

427 at 4C for 10 minutes. Concentration of both cellular and tissue protein extracts was

428 determined by BCA assay (Pierce).

429

430 *Immunodetection of proteins*

431 The localization of proteins by immunofluorescence in fixed MEF cells was performed

432 as described previously [10]. The following antibodies were used: rabbit anti-TOM20

433 (Santa Cruz Biotechnology, sc-11415, 1:200), Alexa Fluor 647 anti-rabbit (Abcam,

434 ab150079, 1:1000), mouse anti-FLAG (Sigma, F1804, 1:1000), Alexa Fluor 594 anti-

435 mouse (Life Technologies, R37121, 1:1000), rat anti-HA (Roche, 11867431001, 1:200),

436 Alexa Fluor 488 anti-rat (Life Technologies, A11006). Immunofluorescence images were

437 captured using a Zeiss LSM880 confocal microscope and processed using ImageJ.

438

439 Detection of proteins by western blotting was achieved by resolving 20-100 µg of

440 extracted protein on SDS-PAGE 4-12% Bis-Tris Bolt gels. These were transferred to

441 nitrocellulose using an iBlot 2 transfer cell (Life Technologies). Antibodies used for

442 western blotting in this work: rat anti-HA (Roche, 11867431001, 1:500), goat anti-rat

443 HRP (Santa Cruz, SC2065, 1:1000). Gels were stained for loading using Coomassie

444 Brilliant Blue (Life Technologies).

445

446

447   *Tissue histology and fluorescence microscopy*

448   To evaluate GFP expression in histological sections, mouse tissues (heart, liver, brain,

449   kidney and skeletal muscles) were snap-frozen in isopentane pre-cooled in liquid

450   nitrogen. Eight μm-thick sections on positive-charged glass slides were fixed in 4%

451   PFA, washed with PBS and finally mounted with Prolong Diamond Antifade Mountant

452   with DAPI. Images were acquired using a Zeiss Axio Observer Z1 microscope LSM 880

453   confocal module, equipped with an Argon Ion MultiLine Laser, Solid State Diode Laser

454   (405 nm), AOTF filter, and a Plan-Apochromat 63x/1.4 NA oil immersion objective). All

455   settings were preserved during image acquisition for all samples. Image J was used to

456   process the images.

457

458   *DNA extraction and quantitation*

459   DNA was extracted from both cultured cells and whole tissues using a Qiagen DNEasy

460   Blood & Tissue kit, according to the manufacturer's instructions. Once acquired, DNA

461   concentrations were assessed by spectrophotometry.

462

463   *Pyrosequencing and qPCR*

464   Assessment of m.5024C>T mtDNA heteroplasmy was carried out by pyrosequencing.

465   PCR reactions for pyrosequencing were prepared using KOD DNA polymerase (Takara)

466   for 40 cycles using 100 ng template DNA with the following primers:

467

468   m.4,962 – 4,986 Forward

469   5' ATACTAGTCCGCGAGCCTTCAAAG 3'

470

471 m.5,360 – m.5,383 Reverse

472 5' [Btn] GAGGGTTCCGATATCTTTGTGATT 3'

473

474 m.5003 – m.5022 Sequencing primer

475 5' AAGTTTAACTTCTGATAAGG 3'

476

477 Mitochondrial DNA copy number of mouse heart samples was determined by qPCR

478 using PowerUp SYBR Green Master Mix according to the manufacturer's protocol

479 (Applied Biosystems). Samples were analysed using a 7900HT Fast Real-Time PCR

480 System (Thermo Fisher). The following primers were used:

481

482 *MT-COI* Forward

483 5' TGCTAGCCGCAGGCATTACT 3'

484

485 *MT-COI* Reverse

486 5' CGGGATCAAAGAAAGTTGTGTTT 3'

487

488 *RNaseP* Forward

489 5' GCCTACACTGGAGTCCGTGCTACT 3'

490

491 *RNaseP* Reverse

492 5' CTGACCACACACGAGCTGGTAGAA 3'

493

494 All primers for pyrosequencing and qPCR were designed using NCBI reference

495 sequences GRCm38.p6 and NC_005089.1 for the C57BL/6j mouse nuclear and

496 mitochondrial genomes respectively.

497

498 *Amplicon resequencing of nuclear DNA off-target sites*

499 Two regions of the NCBI reference sequence for C57BL/6j nuclear DNA demonstrated

500 significant homology (>75% sequence identity) with the mtZFN target site in mtDNA.

501 Amplicons containing these sites were obtained by PCR using primers listed below:

502

503 *Ch.2 Forward*

504 5' GGGTTCCGATATCTTTGTGATTGG 3'

505

506 *Ch.2 Reverse*

507 5' GAGCATAAGCCATTGTTGTTCTG 3'

508

509 *Ch.5 Forward*

510 5' GACTACCTGAGCAAGGAGTC 3'

511

512 *Ch.5 Reverse*

513 5' CTACAGGAGATGGAGGACAC 3'

514

515 All primers were designed using NCBI reference sequence GRCm38.p6 for the

516 C57BL/6j mouse nuclear genome. PCR amplicons were subjected to Nextera sample

517 processing, and resulting libraries were assessed by 2 x 150-cycle paired-end

518 sequencing using a MiSeq instrument (Illumina). Quality trimming and 3'-end adapter

519 clipping of sequenced reads were performed simultaneously with Trim Galore! (--paired)

520 and aligned to GRCm38 using bowtie2. Only reads that contained the entire region

521 chr5: 60042834-60042934 or chr2: 22589909-22590009 were selected for counting with

522   SAMtools (flagstat) and insertion/deletion count based on CIGAR string (I/D). All

523   individual samples yielded >10,000 reads per nucleotide.

524

525   *Amplicon resequencing of the mtDNA target site*

526   The region m.4,962 - 5,383, also used for pyrosequencing analysis, was amplified by

527   PCR using un-biotinylated primers. PCR amplicons were subjected to Nextera sample

528   processing, and resulting libraries were assessed by 2 x 150-cycle paired-end

529   sequencing using a MiSeq instrument (Illumina). Quality trimming and 3'-end adapter

530   clipping of sequenced reads were performed simultaneously with Trim Galore! (--paired)

531   and aligned to GRCm38 using bowtie2. Only reads that contained the entire region

532   m.4,994 – 5,094 were selected for counting with SAMtools (flagstat) and

533   insertion/deletion count based on CIGAR string (I/D). All individual samples yielded

534   >10,000 reads per nucleotide.

535

536   *RNA extraction and northern blotting*

537   Total RNA was extracted from 25 mg of mouse heart tissue using Trizol (Ambion) by

538   homogenization using a gentleMACS dissociator (Miltenyi). Northern blotting was

539   performed as described previously [31]. Briefly, 5 μg of total RNA was resolved on a 10 %

540   (w/v) polyacrylamide gel containing 8 M urea. Gels were dry blotted onto a positively

541   charged nylon membrane (Hybond-N+), with the resulting membrane cross-linked by

542   exposure to 254 nm UV light, 120 mJ/cm2. For tRNA probes, cross-linked membranes

543   were hybridised with radioactively labelled RNA probes T7 transcribed from PCR

544   fragments corresponding to appropriate regions of mouse mtDNA. 5S rRNA was probed

545   with a complementary $\alpha[^{32}P]$-end labelled DNA oligo. Membranes were exposed to a

546   storage phosphor screen and scanned using a Typhoon phosphor imaging system (GE

547   Healthcare). The signals were quantified using Fiji software. The following

548   primers/oligonucleotides were used:

549

550   *MT-TA* Forward

551   5' TAATACGACTCACTATAGGGAGACTAAGGACTGTAAGACTTCATC 3'

552

553   *MT-TA* Reverse

554   5' GAGGTCTTAGCTTAATTAAAG 3'

555

556   *MT-TC* Forward

557   5' TAATACGACTCACTATAGGGAGACAAGTCTTAGTAGAGATTTCTC 3'

558

559   *MT-TC* Reverse

560   5' GGTCTTAAGGTGATATTCATG 3'

561

562   *MT-TL*1 Forward

563   5' TAATACGACTCACTATAGGGAGACTATTAGGGAGAGGATTTGAAC 3'

564

565   *MT-TL1* Reverse

566   5' ATTAGGGTGGCAGAGCCAGG 3'

567

568   5S rRNA oligo:

569   5' AAGCCTACAGCACCCGGTATTCCCAGGCGGTCTCCCATCCAAGTACTAACCA 3'

570

571   All primers for northern blotting were designed using NCBI reference sequences

572   GRCm38.p6 and NC_005089.1 for the C57BL/6j mouse nuclear and mitochondrial

573   genomes respectively.

574

575   *Sample preparation and liquid chromatography coupled to mass spectrometry (LC-MS)*

576   *analysis*

577   Snap-frozen tissue specimens were cut and weighed into Precellys tubes prefilled with

578   ceramic beads (Stretton Scientific Ltd., Derbyshire, UK). An exact volume of extraction

579   solution (30% acetonitrile, 50% methanol and 20% water) was added to obtain 40 mg

580   specimen per mL of extraction solution. Tissue samples were lysed using a Precellys 24

581   homogenizer (Stretton Scientific Ltd., Derbyshire, UK). The suspension was mixed and

582   incubated for 15 minutes at 4°C in a Thermomixer (Eppendorf, Germany), followed by

583   centrifugation (16,000 g, 15 min at 4°C). The supernatant was collected and transferred

584   into autosampler glass vials, which were stored at -80°C until further analysis. Samples

585   were randomized in order to avoid bias due to machine drift and processed blindly. LC-

586   MS analysis was performed using a QExactive Orbitrap mass spectrometer coupled to

587   a Dionex U3000 UHPLC system (Thermo). The liquid chromatography system was

588   fitted with a Sequant ZIC-pHILIC column (150 mm × 2.1 mm) and guard column (20 mm

589   × 2.1 mm) from Merck Millipore (Germany) and temperature maintained at 40°C. The

590   mobile phase was composed of 20 mM ammonium carbonate and 0.1% ammonium

591   hydroxide in water (solvent A), and acetonitrile (solvent B). The flow rate was set at 200

592   µL/min with the gradient as described previously [32]. The mass spectrometer was

593   operated in full MS and polarity switching mode. The acquired spectra were analyzed

594   using XCalibur Qual Browser and XCalibur Quan Browser software (Thermo Scientific).

595

596

597 *Statistical analysis*

598 One and two-tailed Student's t-test were used to compare independent means.

599 Statistical analysis was performed using Prism 5 software.
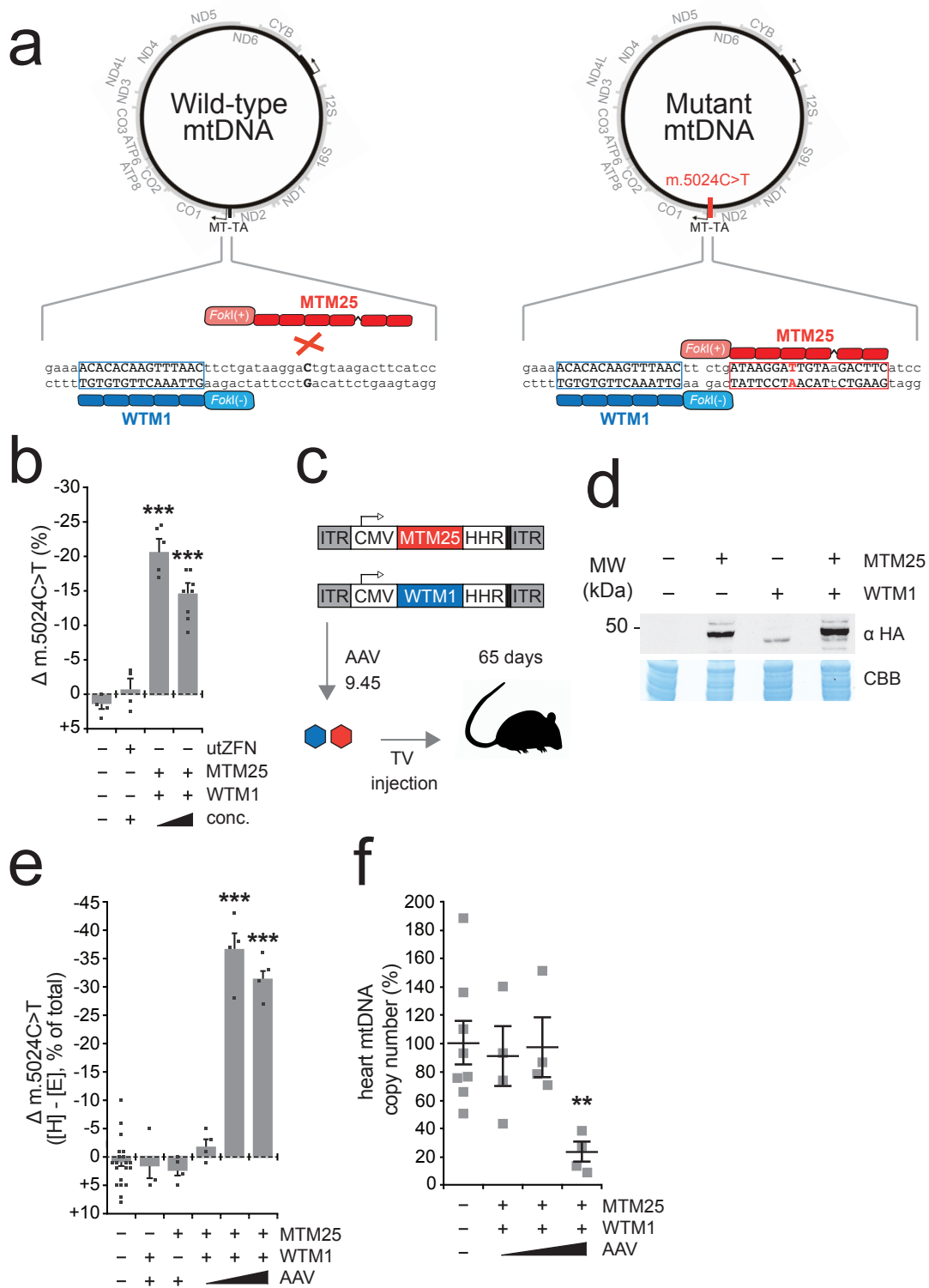
600

601 [Methods-only References]

602 30   Beilstein, K., Wittmann, A., Grez, M. & Suess, B. Conditional control of
603   mammalian gene expression by tetracycline-dependent hammerhead ribozymes.
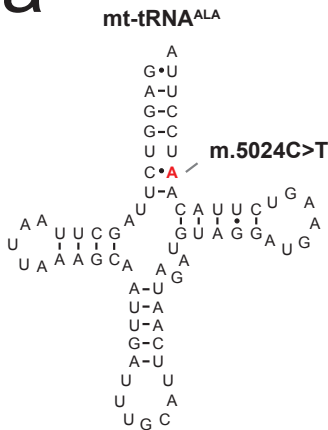604   *ACS Synth Biol* **4**, 526-534, doi:10.1021/sb500270h (2015).
605 31   Pearce, S. F. *et al.* Maturation of selected human mitochondrial tRNAs requires
606   deadenylation. *Elife* **6**, doi:10.7554/eLife.27596 (2017).
607 32   Mackay, G. M., Zheng, L., van den Broek, N. J. & Gottlieb, E. Analysis of Cell
608   Metabolism Using LC-MS and Isotope Tracers. *Methods Enzymol* **561**, 171-196,
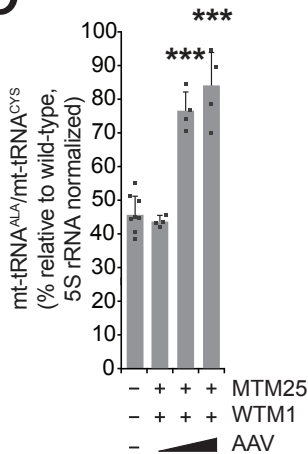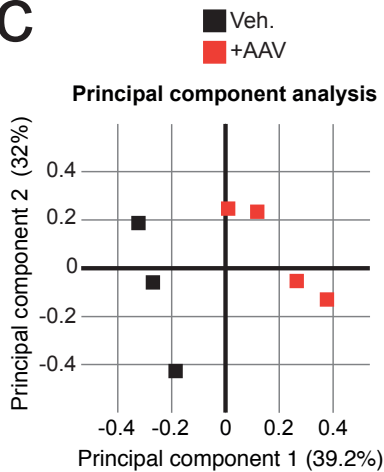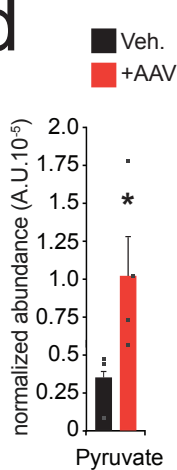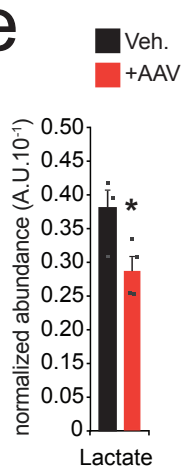609   doi:10.1016/bs.mie.2015.05.016 (2015).
610

Figure 1 - Gammage et al

a

Wild-type mtDNA

Mutant mtDNA

m.5024C>T

b

c

d

e

f

Figure 2 - Gammage et al